CFD Modeling and Validation of the Turbulent Fluidized Bed of FCC Particles

Jinsen Gao, Xingying Lan, Yiping Fan, Jian Chang, Gang Wang, Chunxi Lu, and Chunming Xu
State Key Laboratory of Heavy Oil Processing, China University of Petroleum, Beijing, 102249, P.R. China

DOI 10.1002/aic.11824
Published online May 18, 2009 in Wiley InterScience (www.interscience.wiley.com).

An experimental and computational study is presented on the hydrodynamic characteristics of FCC particles in a turbulent fluidized bed. Based on the Eulerian/Eulerian model, a computational fluid dynamics (CFD) model incorporating a modified gas-solid drag model has been presented, and the model parameters are examined by using a commercial CFD software package (FLUENT 6.2.16). Relative to other drag models, the modified one gives a reasonable hydrodynamic prediction in comparison with experimental data. The hydrodynamics show more sensitive to the coefficient of restitution than to the flow models and kinetics theories. Experimental and numerical results indicate that there exist two different coexisting regions in the turbulent fluidized bed: a bottom dense, bubbling region and a dilute, dispersed flow region. At low-gas velocity, solid-volume fractions show high near the wall region, and low in the center of the bed. Increasing gas velocity aggravates the turbulent disorder in the turbulent fluidized bed, resulting in an irregularity of the radial particle concentration profile. © 2009 American Institute of Chemical Engineers *AIChE J,* 55: 1680–1694, 2009
Keywords: drag force model, turbulent fluidized bed, FCC particle, Eulerian simulation

Introduction

Fluidization is widely used industrially because of its continuous powder handling ability, vigorous gas-solids contacting, and favorable heat- and mass-transfer characteristics. In some industrial fluidized-bed applications where minimizing entrainment and maximizing gas throughput lead to improved reactor performance, the turbulent fluidization flow regime is a feasible operating mode for applications, e.g., for fluid catalytic cracking (FCC) regenerators, noncatalytic fluidized-bed reactors and particle drying.[1]

Turbulent fluidization has only been widely recognized as a distinct flow regime for the past two decades, occurring between the bubbling and the fast fluidization regimes.[2–6] As the gas velocity is increased from the bubbling regime into the turbulent regime, a different behavior is observed, in particular a diffuse bed surface, turbulent motion of solids clusters and voids of irregular shapes.[7] A turbulent fluidized bed is characterized by two different coexisting regions: a bottom dense, bubbling region and a dilute, dispersed flow region.[2] The second characteristic of the turbulent fluidization is the high value of the dispersion coefficients for the solids. Du et al.[5,8] reported that the dispersion coefficients in the turbulent regime are much higher than in the neighboring flow regimes. Bi et al. [4] presented a comprehensive review of the turbulent fluidization. Much valuable information on turbulent fluidization, such as existence of and transition to turbulent fluidization, gas-solids mixing, heat and mass transfer, solids entrainment in turbulent fluidized beds and modeling and reactor performance, were summarized in that review article; the aspects that need to be advanced in the future were also addressed. Ellis et al.[9] carried out an experimental study of the hydrodynamics of gas-solid turbulent fluidized beds of FCC particles in columns of diameter 0.26, 0.61 and 1.56 m, and the scale-up effects in turbulent fluidized beds were investigated. Relative to the adjacent two flow regimes,

Correspondence concerning this article should be addressed to C. Xu at xcm@cup.edu.cn.

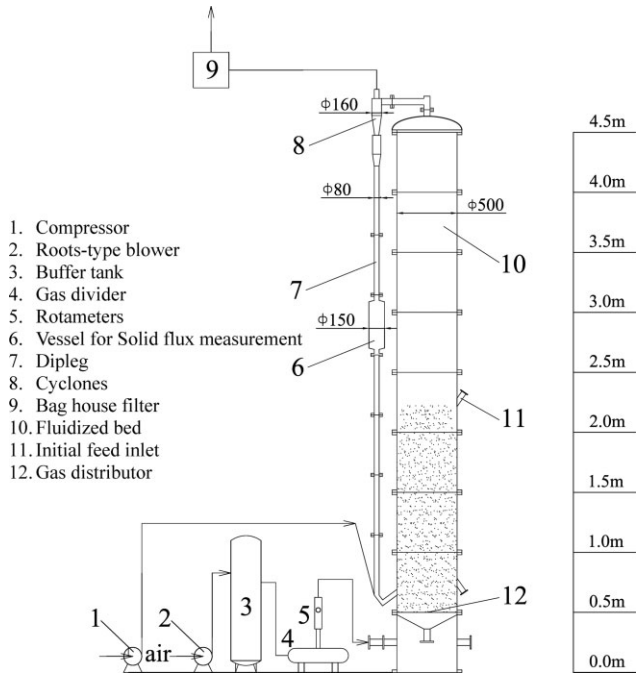

Figure 1. Scheme diagram of experimental apparatus of the turbulent gas-solid fluidized bed.

turbulent fluidization has received much less attention due to the challenges of experimental and theoretical work related to this flow regime.

With the increase of computational power, computational fluid dynamics (CFD) offers a fresh approach to understand the hydrodynamics and transfer mechanisms in multiphase flows. Based on the two-fluid model and a modified gas-solid drag model, a CFD model of turbulent flow has been developed and the hydrodynamics were predicted in the turbulent fluidized bed,[1,10] although receiving much less attention than the adjacent flow regimes of bubbling and fast fluidization. The basic features of this flow regime were thus captured. The profiles of the velocity and volume fraction of the gas and solid phases have been obtained and shown to be in reasonable agreement with the experimental data. Moreover, some items such as granular temperatures, strong anisotropy and frequencies of oscillations, which cannot be obtained or are hard to obtain in laboratory conditions, were easily estimated using CFD tools. The use of CFD in the field of fluidization pushed the frontiers of fundamental understanding of fluid-solid interaction and enabled the correct theoretical prediction of various macroscopic phenomena encountered in fluidized bed.

For the design and optimization of a turbulent fluidized bed reactor, a better understanding of its hydrodynamics is required. For this purpose, a pilot-plant scale gas-solid fluidized bed has been built and the turbulent flow behavior of FCC particle (Geldart Group A) is thus, investigated experimentally. Furthermore, a modified drag model is proposed on the basis of an effective mean diameter of particles clusters together with the bed voidage profile. By incorporating it into a CFD code (FLUENT 6.2.16), an Eulerian/Eulerian two-fluid model for turbulent gas-solid fluidized bed containing FCC particle is developed. The gas-solid flow behaviors in the turbulent fluidized bed are predicted and compared with the experimental data. Comparison of the simulation and experimental results may further validate the feasibility of the CFD model, and subsequently gives insight into the improvement of a turbulent fluidized-bed reactor.

Experimental Apparatus, Materials and Procedure

All experiments of this study are carried out in a plexiglass gas-solid fluidized bed of size 500 mm I.D. and 4 m height, as shown in Figure 1. The fluidized bed is also equipped with a high-pressure drop perforated distributor and cyclones. Fluidizing air flow rates are regulated by a set of rotameters. The pressure profiles within the fluidized bed are measured by the U-tube water manometers together with the DDY-type pressure sensors. Bed heights are measured directly by setting a ruler along the plexiglass bed.

FCC catalyst with a density of 1500 kg/m^3 and Sauter mean diameter of 60 μm is used as the experimental particle. Its properties are reported in Table 1. Air is employed as the fluidization gas. Its density and viscosity are 1.225 kg/m^3 and 1.7×10^{-5} kg/m·s, respectively.

Initially, a certain amount of FCC particles are filled in the fluidized bed with a given bed height. Air is then introduced into the fluidized bed through gas distributor to completely fluidize the FCC particles. During a stable operation, some FCC particles can be entrained and then leave the fluidized bed. After being separated in the cyclone, the solids descend downward through the dipleg and then return to the fluidized bed.

CFD Model for Turbulent Gas-Solid Fluidized Beds

Governing equations

Due to the high particle concentrations in gas-solid turbulent fluidized beds the particle-particle interactions cannot be neglected. Moreover, the solid phase has similar properties to a continuous fluid. By using the kinetic theory of granular flows,[11,12] the viscous forces and the solid pressure of the particulate phase can be described as a function of the so-called granular temperature. Therefore, the Eulerian model using the kinetic theory for granular flow has shown its suitability for modeling dense gas-solid fluidized bed reactors.

In this article, a commercial CFD package (FLUENT6.2.16)[13] is used to carry out the simulation work, and the governing equations in Eulerian notation are given in Table 2.

Drag laws for turbulent fluidized beds of FCC particles

β in the momentum equation is the interphase drag coefficient between the gas and FCC particle phase, which is a

Table 1. Properties of Experimental FCC Particle

Size range	μm	20-130
Mean diameter	μm	60
Particle density	kg/m^3	1500
Minimum fluidization velocity	m/s	0.0047
Terminal velocity	m/s	0.58
Geldart Group		A

Table 2. Governing Equations

Gas-phase continuity equation	$\frac{\partial(\alpha_g\rho_g)}{\partial t}+\frac{\partial}{\partial x_j}(\alpha_g\rho_g u_{gj})=0$
Solid-phase continuity equation	$\frac{\partial(\alpha_p\rho_p)}{\partial t}+\frac{\partial}{\partial x_j}(\alpha_p\rho_p u_{pj})=0$
	$\alpha_p+\alpha_g=1$
Gas-phase momentum equation	$\frac{\partial}{\partial t}(\alpha_g\rho_g u_{gi})+\frac{\partial}{\partial x_j}(\alpha_g\rho_g u_{gi}u_{gj})=-\alpha_g\frac{\partial p}{\partial x_i}+\frac{\partial\tau_{g,ij}}{\partial x_j}-\beta(u_{gi}-u_{pi})+\rho_g\alpha_g g_i$
Solid-phase momentum equation	$\frac{\partial}{\partial t}(\alpha_p\rho_p u_{pi})+\frac{\partial}{\partial x_j}(\alpha_p\rho_p u_{pi}u_{pj})=-\alpha_p\frac{\partial p}{\partial x_i}+\frac{\partial\tau_{p,ij}}{\partial x_j}-\beta(u_{pi}-u_{gi})+\rho_p\alpha_p g_i$
Solid-phase turbulent fluctuating energy equation	$\frac{3}{2}\left[\frac{\partial(\alpha_p\rho_p\Theta)}{\partial t}+\frac{\partial(\alpha_p\rho_p u_{pk}\Theta)}{\partial x_k}\right]=\frac{\partial}{\partial x_k}\left(\Gamma_\Theta\frac{\partial\Theta}{\partial x_k}\right)+\mu_p\left(\frac{\partial u_{pk}}{\partial x_i}+\frac{\partial u_{pi}}{\partial x_k}\right)\frac{\partial u_{pk}}{\partial x_i}-p_p\frac{\partial u_{pk}}{\partial x_k}+\left(\xi_p-\frac{2}{3}\mu_p\right)\left(\frac{\partial u_{pk}}{\partial x_k}\right)^2-\gamma$
Gas-phase stress tensor	$\tau_{g,ij}=\mu_g\left(\frac{\partial u_{gj}}{\partial x_i}+\frac{\partial u_{gi}}{\partial x_j}\right)$
Solid-phase stress tensor	$\tau_{p,ij}=\mu_p(\frac{\partial u_{pj}}{\partial x_i}+\frac{\partial u_{pi}}{\partial x_j})+(\xi_p-\frac{2}{3}\mu_p)\frac{\partial u_{pk}}{\partial x_k}\delta_{ij}-p_p\delta_{ij}$
Solid-phase pressure	$p_p=\alpha_p\rho_p[1+2(1+e)\alpha_p g_0]\Theta$
Radial distribution function	$g_0=[1-(\frac{\alpha_p}{\alpha_{p,max}})^{\frac{1}{3}}]^{-1}$
Granular temperature	$\Theta=\frac{1}{3}<\overline{u'_p u'_p}>$
Solids phase shear viscosity (Gidaspow kinetic theory[14])	$\mu_p=\frac{10\rho_p d_p\sqrt{\pi\Theta}}{96(1+e)g_0}\left[1+\frac{4}{5}(1+e)g_0\alpha_p\right]^2+\frac{4}{5}\alpha_p^2\rho_p d_p g_0(1+e)\sqrt{\frac{\Theta}{\pi}}$
Solids phase shear viscosity (Syamlal-O'Brien kinetic theory[15])	$\mu_p=\frac{\alpha_p\rho_p d_p\sqrt{\pi\Theta}}{6(3-e)}\left[1+\frac{2}{5}(1+e)(3e-1)g_0\alpha_p\right]^2+\frac{4}{5}\alpha_p^2\rho_p d_p g_0(1+e)\sqrt{\frac{\Theta}{\pi}}$
Solids bulk viscosity	$\xi_p=\frac{4}{3}\alpha_p^2\rho_p d_p g_0(1+e)\sqrt{\frac{\Theta}{\pi}}$
Diffusion coefficient (Gidaspow kinetic theory[14])	$\Gamma_\Theta=\frac{150\rho_p d_p\sqrt{\pi\Theta}}{384(1+e)g_0}[1+\frac{6}{5}(1+e)g_0\alpha_p]^2+2\alpha_p^2\rho_p d_p g_0(1+e)\sqrt{\frac{\Theta}{\pi}}$
Diffusion coefficient (Syamlal-O'Brien kinetic theory[15])	$\Gamma_\Theta=\frac{15\alpha_p\rho_p d_p\sqrt{\pi\Theta}}{4(41-\frac{33}{2}(1+e))}[1+\frac{3}{5}(1+e)^2(2e-1)g_0\alpha_p+\frac{8}{15\pi}(41-\frac{33}{2}(1+e))(1+e)\alpha_p g_0]$
Collisional dissipation of energy fluctuation	$\gamma=3(1-e^2)\alpha_p^2\rho_p g_0\Theta\left[\frac{4}{d_p}\sqrt{\frac{\Theta}{\pi}}-\frac{\partial u_{pk}}{\partial x_k}\right]$

key parameter for the successful simulation of the hydrodynamics in a turbulent fluidized bed.

Several drag models have been developed to express the interactions between the particles and the gas in fluidized bed based on packed-bed measurements,[16] settling experiments,[17,18] and fluidized-bed experiments.[19] Many researchers have successfully performed circulating fluidized beds simulations of FCC particles or bubbling fluidized-bed simulations of the more coarse Geldart B particles with various model validations. However, there are few successful simulations reported on the bubbling or turbulent beds of Geldart A particles.[20,21] They always observed severe overestimation of bed expansion in the bubbling bed and underestimation of bed density in the turbulent bed, respectively. McKeen and Pugsley[21] reported that the generally poor simulation results for Geldart A particles can be attributed to the existence of significant interparticle forces due to the van der Waals attraction. The existence of cohesive interparticle forces would lead to grouping of particles, resulting in larger effective particle sizes, and hence reduced fluid-particle drag forces.

Qi et al.[22] claimed that the present drag correlations were suitable only for lower gas velocities and coarse particles, in which case the terminal velocity was equal or close to the superficial gas velocity. O'Brien and Syamlal[23] also reported that these drag correlations must be corrected to account for cluster effects for fine particles (Geldart A particle). For this reason, some modifications on the gas-solid drag force model have been proposed to accounting for the aggregation of FCC particles due to the interparticle forces. Syamlal and O'Brien[18] introduced a method to modify their drag law based on the experimental pressure drop data and the minimum fluidization velocity of the particles by adjusting the model parameter of P and Q. This model was reported to be reasonable for finding suitable values for the drag adjustment, when applied to a bubbling fluidized bed of FCC particles.[24,25]

Considering the critical effect of the particle clusters or strands on the drag coefficient, Yang et al.[26,27] presented a drag model based on the energy-minimization multiscale (EMMS) approach. With that drag correlation, the dynamic formation and dissolution of the clusters can be predicted,

Table 3. Flow Zones Classification and its Drag Force Correlation

Void fraction	Drag force model	Drag force coefficient
≤ 0.80	Ergun	$\beta_1 = 150\frac{\alpha_p(1-\alpha_g)\mu_g}{\alpha_g(d_p^*)^2} + 1.75\frac{\rho_g\alpha_p\lvert\vec{u}_p-\vec{u}_g\rvert}{d_p^*}$
0.8-0.933	ZP	$\beta_2 = \frac{5}{72}C_D\frac{\alpha_p\alpha_g\rho_g\lvert\vec{u}_p-\vec{u}_g\rvert}{d_p^*(1-\alpha_g)^{0.293}}$
		$C_D = \begin{cases}\frac{24}{Re_p^*}(1+0.15Re_p^{*0.687}) & (Re_p^* \leq 1000)\\ 0.44 & (Re_p^* > 1000)\end{cases}$
		$Re_p^* = \frac{\alpha_g\rho_g d_p^*\lvert\vec{u}_g-\vec{u}_p\rvert}{\mu_g}$
0.933-0.990	Wen & Yu	$\beta_3 = \frac{3}{4}C_D\frac{\alpha_p\alpha_g\rho_g\lvert\vec{u}_p-\vec{u}_g\rvert}{d_p}\alpha_g^{-2.65}$
0.990-1.00	Schiller & Naumann	$\beta_4 = \frac{3}{4}C_D\frac{\alpha_p\rho_g\lvert\vec{u}_p-\vec{u}_g\rvert}{d_p}$
		$C_D = \begin{cases}\frac{24}{Re_p}(1+0.15Re_p^{0.687}) & (Re_p \leq 1000)\\ 0.44 & (Re_p > 1000)\end{cases}$
		$Re_p = \frac{\alpha_g\rho_g d_p\lvert\vec{u}_p-\vec{u}_g\rvert}{\mu_g}$

which suggests the feasibility of the EMMS approach to be used as a subgrid closure law for drag coefficient. Using the EMMS approach,[1] the CFD model with a drag corrected for clusters achieved the basic features of the turbulent fluidized bed of FCC particles: the dilute and dense regions, high-dispersion coefficients and a strong anisotropy. However, the simulation with the EMMS drag overpredicted the solid volume fractions at the bottom of the bed by a factor of about three.

McKeen and Pugsley[21,28] and Sharma et al.[29] also proposed an empirical method to reduce the Gibilaro drag correlation[30] using a constant scale factor. The scale factor could be adjusted to take into account the effect of interparticle cohesive forces on particle agglomeration. McKeen and Pugsley[21,28] found that the Gibilaro drag model[30] with a correction factor of 0.25, corresponding to an effective particle agglomerate diameter in the range of 135 to 170 μm for FCC particles of actual 75 μm mean diameter, could adequately predict the bubbling fluidization behavior observed experimentally.

The idea of using an effective agglomerate or cluster diameter for FCC particles has existed for some time. Arastoopour and Gidaspow[31] defined an effective cluster diameter to fit their one-dimensional (1-D) hydrodynamic FCC riser model to experimental data. Recently, Lettieri et al.[32] analyzed the homogeneous expansion data for FCC particles in terms of the Richardson-Zaki equation. In air at 20°C, the experimentally obtained terminal velocity, u_t^*, is much higher than the calculated one (u_t). If a homogeneous bed was assumed to be characterized by the presence of clusters, the diameter of the cluster, d_p^*, can be back-calculated from the experimental u_t^* values. Lettieri et al.[32] also calculated effective cluster diameters in the range of 200 to 474 μm for FCC catalysts with Sauter mean diameters from 49 to 71 μm in their work.

Based on the aforementioned research, an effective mean diameter of 300 μm (d_p^*, the diameter of particle clusters) is obtained instead of the actual 60 μm FCC particle to modify this drag force model in this work. This modification combines the influence of interparticle forces, and hence the effect of particle agglomeration on the drag force.

In addition, as aforementioned, when the gas velocity increases from the bubbling regime into the turbulent regime, turbulent motion of solids clusters and voids of irregular shapes are observed. A turbulent fluidized bed is characterized by two different coexisting regions: a bottom dense, bubbling region and a dilute, dispersed flow region.[2] The gas-solid drag force is intrinsically dependent on the bubble motion and void profiles of a fluidized bed. According to the turbulent flow behavior of FCC particles and void fraction profile observed in experiment, four zones (dense phase, subdense phase, subdilute phase, and dilute phase zone) can be identified in a turbulent fluidized bed. The void fraction of 0.933, corresponding to the bed density of about 100 kg/m^3, can be used as the dividing criteria for the dense and dilute phase. In the dense phase zone ($\alpha_g \leq 0.80$) and subdense phase zone ($0.8 < \alpha_g \leq 0.933$), the Ergun drag model[16] and the ZP drag model[10] modified with effective mean diameter of 300 μm are used, respectively. The ZP drag model used in this work is based on the modification of the drag coefficient for a single particle (C_D), with a correction function ($f(\alpha_g) = \frac{1}{10.8(1-\alpha_g)^{0.293}}$) proposed by Matsen.[33,34] In the dilute phase zone ($0.990 < \alpha_g \leq 1.00$) and subdilute phase zone ($0.933 < \alpha_g \leq 0.990$), the Schiller and Naumann[35] and the Wen and Yu drag model[19] are employed, respectively. These drag force correlations are summarized in Table 3.

To avoid discontinuity of these equations, Lu et al.[36] introduced a switch function that gave a smooth but rapid transition from one regime to the other

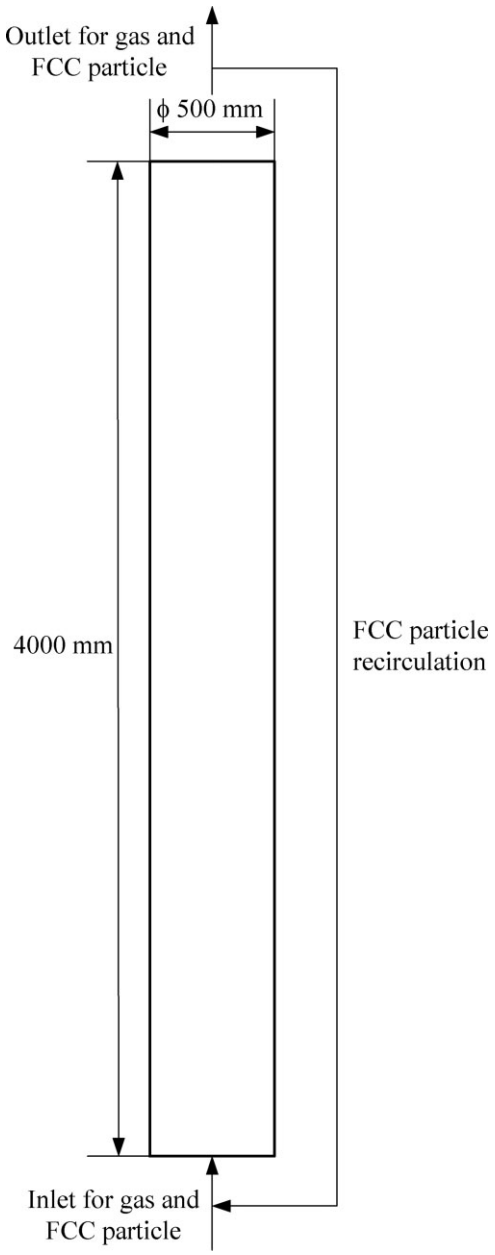

Figure 2. Geometry of the simulation system.

$$\varphi_i = \frac{\arctan[150 \times 1.75(\alpha_g - \alpha_i)]}{\pi} + 0.5 \quad (1)$$

where, α_i corresponds to the void fraction for the dividing criteria, i.e., 0.80, 0.933 and 0.99. Thus, the gas-particle interaction coefficient is given by

$$\beta = (1-\varphi_1)\beta_1 + \varphi_1\{(1-\varphi_2)\beta_2 + \varphi_2[(1-\varphi_3)\beta_3 + \varphi_3\beta_4]\} \quad (2)$$

Simulation Method

Simulation code and numerical algorithm

Differential equations mentioned in the previous section are solved by a finite volume method (FVM). These equations are discretized by an upwind differencing scheme over the used finite volume, and solved by the commercial CFD code (FLUENT 6.2.16). The solution of the pressure from the gas phase momentum equation requires a pressure correction equation that adjusts the pressure and the velocities after each iteration of discretized momentum equations. In this work, the popular SIMPLE algorithm by Patankar[37] is used for this purpose.

Each simulation is performed up to 30 s of real-time. The time-averaged distributions of variables are computed covering a period of 25-30 s.

Simulation systems

All simulations are performed in 2-D Cartesian space. The dimensions of the computational domain in radial and axial directions are same to those of the actual fluidized bed in the experimental apparatus. The structures of the simulation system are shown in Figure 2.

Grids are created in a CAD program called GAMBIT 2.2.30 and exported into FLUENT 6.2.16. The structured mesh is implemented with 100 × 194 grids (radial × axial). In addition, the meshes with 40 × 89, 50 × 144, and 200 × 420 grids are also used to confirm the mesh independency.

Boundary and initial conditions

Inlet at the bed bottom is designated as Velocity Inlet boundary conditions for both the gas and solid phases, where the direction of gas or particle flow is normal to the surface. The boundary condition at the top of the bed is a pressure boundary fixed at a reference value (atmospheric). Solids are free to leave if entrained and then return to the computational domain from the bottom inlet with a same mass flux. Everywhere else are boundary conditions specified as Wall, which are all set as no-slip wall boundary condition for both the gas and solid phases.

FCC particle is used as the solid-phase. Air is employed to fluidize FCC particles, with a density of 1.225 kg/m^3. At the bottom of the bed, the gas velocity is given. The inlet gas velocities range form 0.2 to 0.7 m/s. Most of the CFD

Table 4. Simulation Parameters used in FLUENT 6.2.16

Flow type	Laminar
Gas-solid model	Eulerian-Eulerian, with kinetic theory
Wall boundary condition	No slip
Time step used	0.0001 s
Max. number of iterations per time step	20
Convergence criteria	10^{-3}
Pressure velocity coupling	SIMPLE
Underrelaxation factors	0.5 for pressure, 0.4 for momentum and 0.2 for volume and granular temperature
Maximum solid packing volume fraction	0.63
Discretization scheme	Second-order upwind
Outlet condition	Atmosphere pressure
Air density	1.225 kg/m^3
Air viscosity	1.7894×10^{-5} kg/(m·s)
FCC particle density	1500 kg/m^3
FCC particle diameter	60 μm
Superficial gas velocity	0.2-0.7 m/s

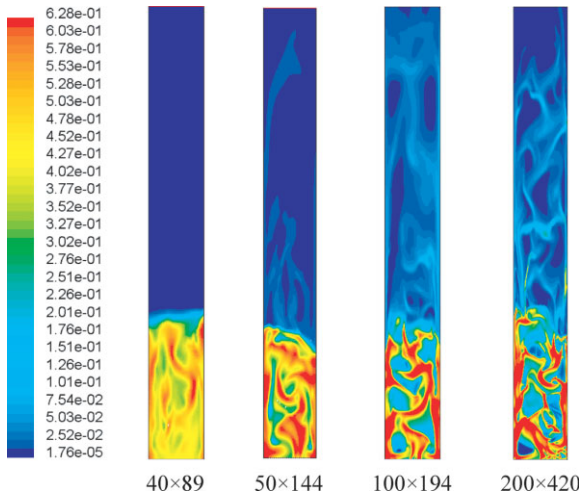

Figure 3. Instantaneous solid volume fractions for various mesh resolutions (u_g = 0.5 m/s).

[Color figure can be viewed in the online issue, which is available at www.interscience.wiley.com.]

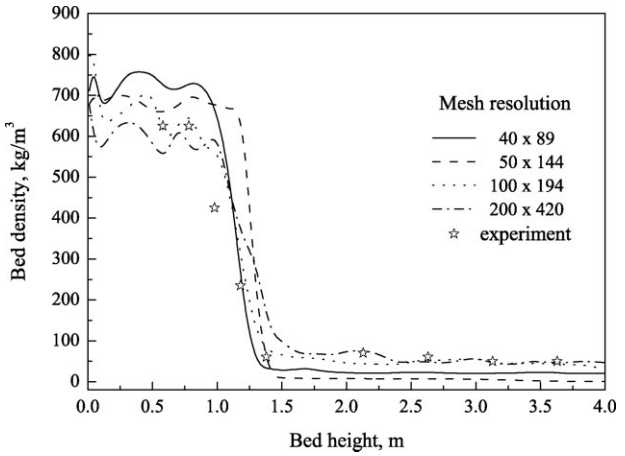

Figure 4. Time-averaged bed density profile for various mesh resolutions (u_g = 0.5 m/s).

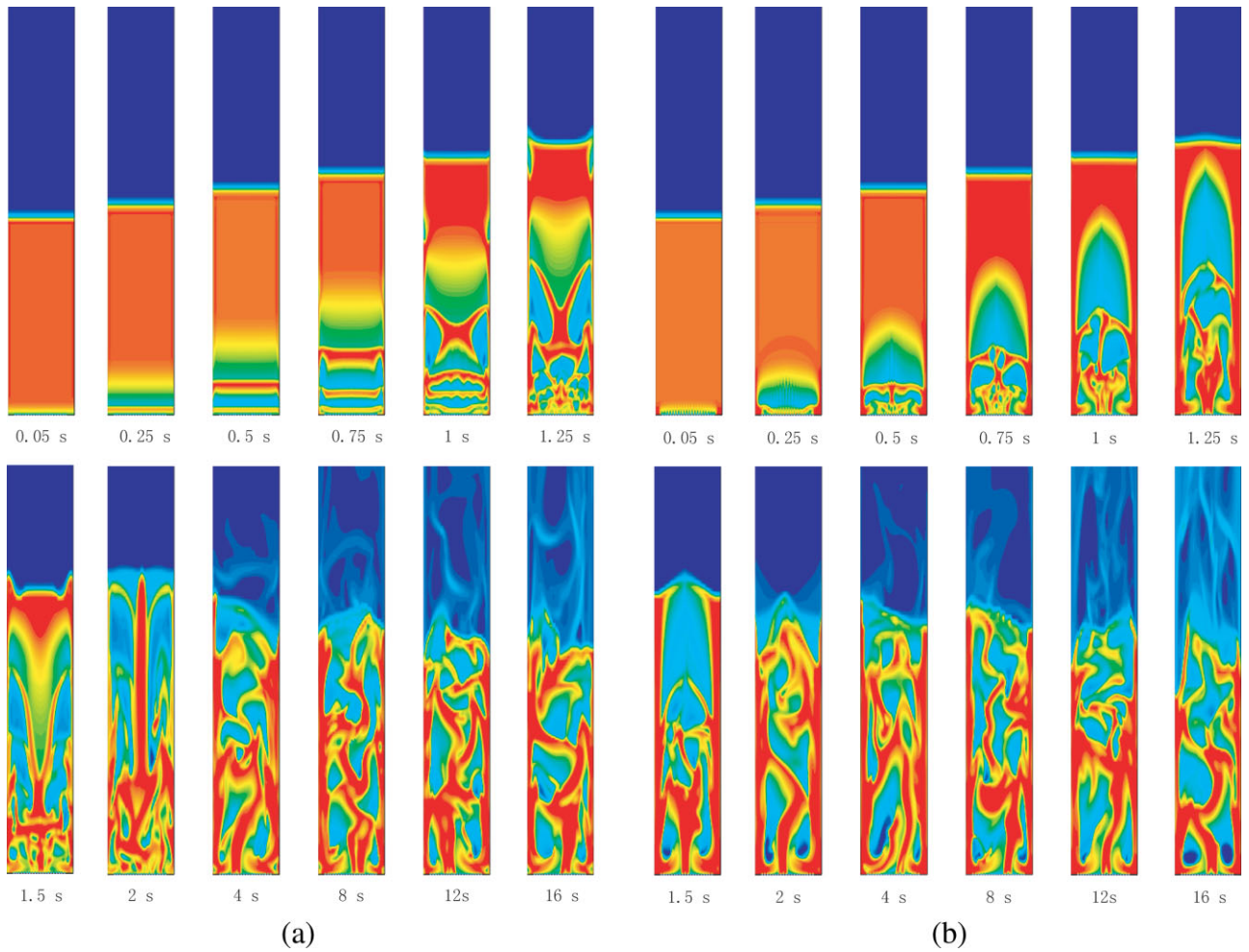

Figure 5. (a) The formation and motion of bubbles in the turbulent fluidized bed (opening ratio of 100%, u_g = 0.5 m/s). (b) The formation and motion of bubbles in the turbulent fluidized bed (opening ratio of 40%, u_g = 0.5 m/s). (c) The formation and motion of bubbles in the turbulent fluidized bed (opening ratio of 10%, u_g = 0.5 m/s).

[Color figure can be viewed in the online issue, which is available at www.interscience.wiley.com.]

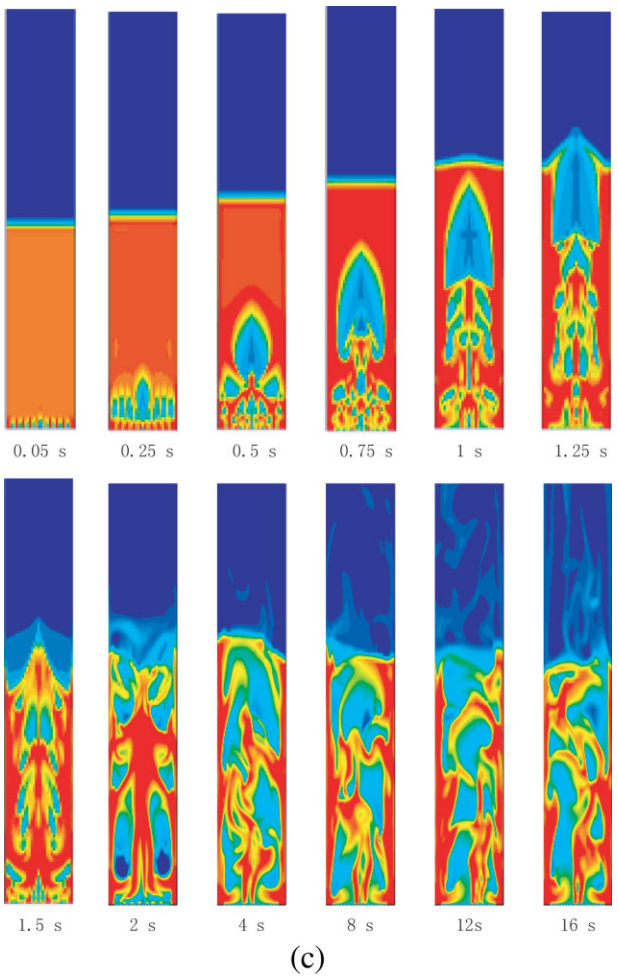

Figure 5. (Continued)

simulations in this study are performed under the same conditions as experiments.

Initially, a certain amount of FCC particles are filled within the bed with a given solid volume fraction and bed height corresponding to the experiment case. The initial velocity of the solid-phase was set to be zero. Table 4 summarizes the numerical parameters for the simulations.

Results and Discussion

Grid independency

No numerical simulation is complete without a study of grid-size dependence. To confirm that the CFD results are independent of the mesh size, the simulations of the system with 40 × 89, 50 × 144, 100 × 194 and 200 × 420 grids (radial × axial) are performed. Figures 3 and 4 show the instantaneous solid-volume fractions and the time-averaged axial-bed density profile at four mesh resolutions, respectively. The calculation condition is 1.0 m for the initial bed height and 0.5 m/s for the superficial gas velocity.

It can be seen that all simulations predict the correct qualitative behavior, such as the bed expansion and the coexisting dilute and dense phases. Relative to the coarser mesh, the fine mesh (200 × 420) case and medium mesh (100 × 194) case capture the more real flow behavior, such as the voids and the solid phase of irregular shapes. Moreover, the medium mesh case and fine mesh case obtain similar solid-volume fraction distributions, which indicates that the mesh size of 100 × 194 is sufficiently fine for providing reasonably mesh independent results. Therefore, the mesh size of 100 × 194 is selected as a base case and applied in the rest of the article.

Effect of opening of the perforated distributor

The effects of the opening ratio of the perforated distributor on the flow behavior of FCC particle are investigated by numerical simulation. The opening ratios employed are 100%, 40%, 20% and 10%. Since the 2-D structured mesh is implemented in this work, the opening pore is uniform over the bottom cells expect for the case of 100%. The superficial gas velocity used is 0.5 m/s.

Figure 5 shows the formation and motion of bubbles in the turbulent fluidized bed. It can be seen from Figure 5 that the formation and motion of bubbles in the turbulent fluidized are distinctly affected by the opening ratios of the inlet. In

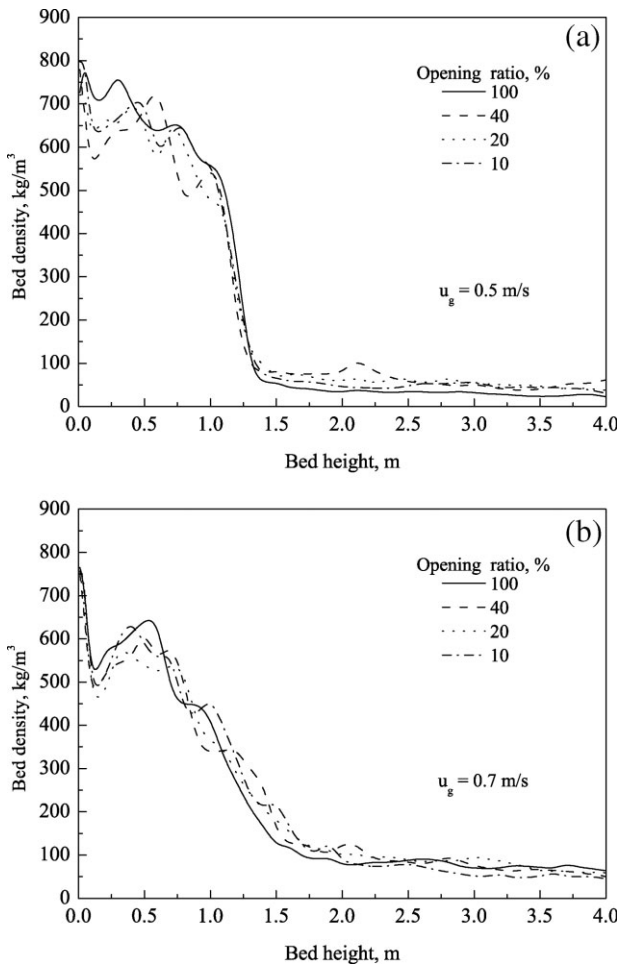

Figure 6. (a) Axial-bed densities profile for various opening ratios of distributors (u_g = 0.5 m/s). (b) Axial-bed densities profile for various opening ratios of distributors (u_g = 0.7 m/s).

Table 5. Summary of the Drag Force Models used for Comparison

Model	Drag force coefficient
Gidaspow	$\beta = 150\frac{\alpha_p(1-\alpha_g)\mu_g}{\alpha_g(d_p)^2} + 1.75\frac{\rho_g\alpha_p\lvert\vec{u}_p-\vec{u}_g\rvert}{d_p} \quad \alpha_g \le 0.8;$
	$\beta = \frac{3}{4}C_D\frac{\alpha_p\alpha_g\rho_g\lvert\vec{u}_p-\vec{u}_g\rvert}{d_p}\alpha_g^{-2.65} \quad \alpha_g > 0.8;$
	$C_D = \begin{cases} \frac{24}{Re_p}(1+0.15Re_p^{0.687}) & (Re_p \le 1000) \\ 0.44 & (Re_p > 1000) \end{cases};$
Syamlal-O'Brien	$\beta = \frac{3\alpha_p\alpha_g\rho_g}{4u_{r,p}^2 d_p}C_D\lvert\vec{u}_p-\vec{u}_g\rvert,$
	$C_D = \left(0.63+\frac{4.8}{\sqrt{Re_p/u_{r,p}}}\right)^2,$
	$u_{r,p} = 0.5\left(A - 0.06Re_p + \sqrt{(0.06Re_p)^2 + 0.12Re_p(2B-A)+A^2}\right),$
	$A = \alpha_g^{4.14};$ if $\alpha_g \le 0.85$, $B = 0.8\alpha_g^{1.28};$ if $\alpha_g > 0.85$, $B = \alpha_g^{2.65}$
Mckeen	$\beta = C\left(\frac{17.3}{Re_p}+0.336\right)\frac{\rho_g\lvert\vec{u}_p-\vec{u}_g\rvert}{d_p}\alpha_p\alpha_g^{-1.8}$
The modified drag model	See Table 3

the cases of opening ratios of 10% and 40%, significant bubble coalescence and split can be observed. Initially, many small bubbles form on the gas distributor. Duo to the coalescence of small bubbles in the bed, bubbles continue to grow up, and rise through the bed. When arriving at the bed surface, bubbles breakup. Big or small bubbles disperse in the bed, which are irregular and elongated. However, bubbles get larger while their number decreases in the case of the opening ratios of 40%, causing the bed expansion increases. In the case of opening ratios of 100%, the bubbles are not as large as in aforementioned case, and also less uniform. In addition, the motion of bubbles is also influenced by the opening ratios, even when the column is truly fluidized.

The predicted axial bed densities are shown in Figure 6 for various opening ratios of distributors. The superficial gas velocities used are 0.5 and 0.7 m/s. It can be seen from Figure 6 that there is no significant difference in the average bed density for different opening ratios of the distributor, since the bed density is a time-average result at a given cross-section.

The aforementioned analysis indicates that at a given gas velocity, the lower the value of opening ratio, the easier the formation of bubbles. The hydrodynamics in the case of opening ratios of 10% is approximately consistent with the experiment. Thus, the inlet configuration with an opening ratio of 10% is used in the next simulation work.

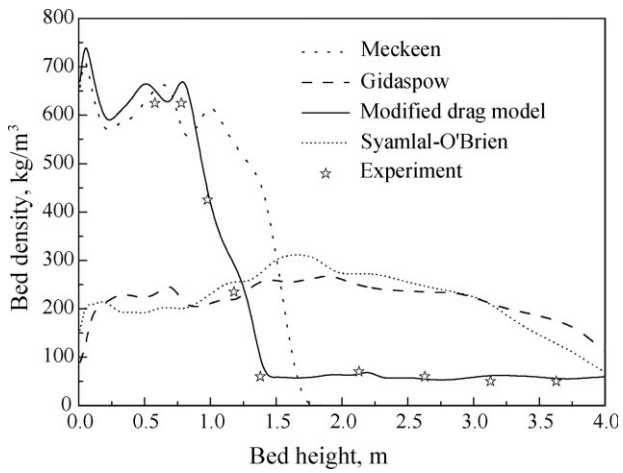

Figure 7. Axial-bed density profiles predicted by various drag models (u_g = 0.5 m/s).

Model Study

Comparison of the modified drag model to other ones

To study the suitability of drag laws for modeling the turbulent fluidization of FCC particles, the modified drag model

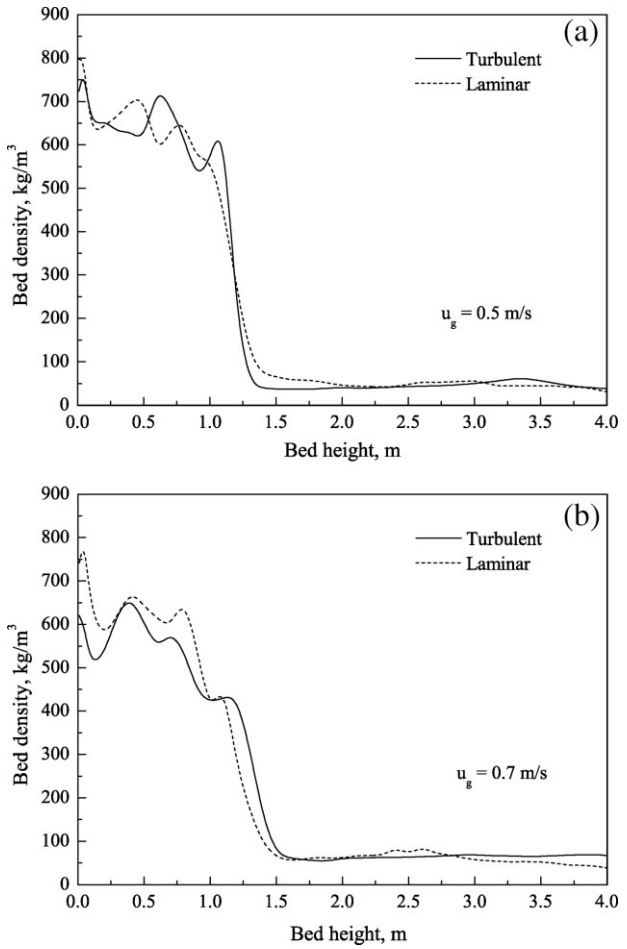

Figure 8. (a) Axial-bed density profile predicted by the laminar model and turbulent model (u_g= 0.5 m/s). (b) Axial-bed density profile predicted by the laminar model and turbulent model (u_g = 0.7 m/s).

and other ones including Gidaspow,[14] Syamlal-O'Brien[15] and McKeen[21] drag model are examined and compared. These drag models are summarized in Table 5. The calculation condition is 1.0 m for the initial bed height and 0.5 m/s for the superficial gas velocity. The predicted axial bed density profiles are shown in Figure 7.

It can be seen that the Gidaspow,[14] Syamlal-O'Brien[15] and McKeen[21] drag model, in its original form, fails to predict the hydrodynamics of FCC particle in a turbulent fluidized bed. All of them did not capture the basic characteristics of turbulent fluidization regime: coexisting the dilute and dense phases. In addition, no significant difference in the fluidization was observed with the Gidaspow and Syamlal-O'Brien drag models: an underestimated bed density in the dense phase, while an overestimated one in the dilute phase of the bed. This should be attributed to the lack of consideration of the effects of cohesive forces and agglomeration, which results in a higher drag force. The McKeen drag model also could not capture the dilute characteristics, although showing a better prediction for the dense phase.

Relative to the Gidaspow,[14] Syamlal-O'Brien[15] and McKeen[21] drag model the modified one gives a reasonable hydrodynamic prediction in comparison to the experimental data of the turbulent fluidized bed, which validates the modified drag model, based on the effective mean diameter of particles cluster together with the bed void fraction profile. Therefore, the modified drag model is employed to investigate the hydrodynamics of the turbulent fluidized bed of FCC particles in the rest of this article.

Laminar model vs. turbulent model

The axial bed density profile predicted by the laminar model and k-ϵ turbulent model for both gas and particle phases are shown in Figure 8 a and b for the gas velocities of 0.5 m/s and 0.7 m/s, respectively. When the k-ϵ turbulent model is applied, the default model parameters in the FLUENT software are employed.

It can be seen that no significant difference was observed in the predicted bed density with these two kinds of flow

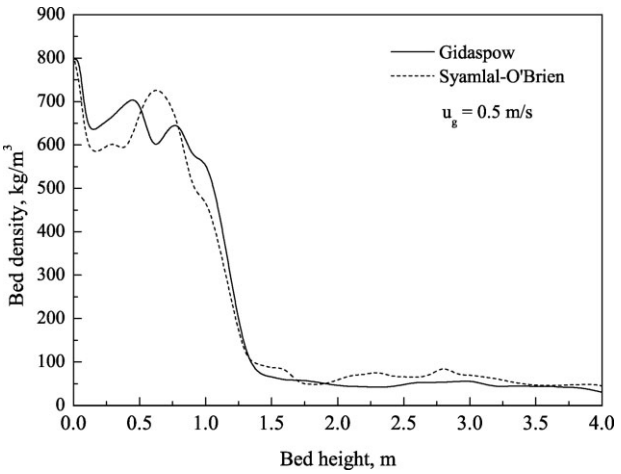

Figure 9. Axial-bed density profile predicted by different kinetic theories (u_g = 0.5 m/s).

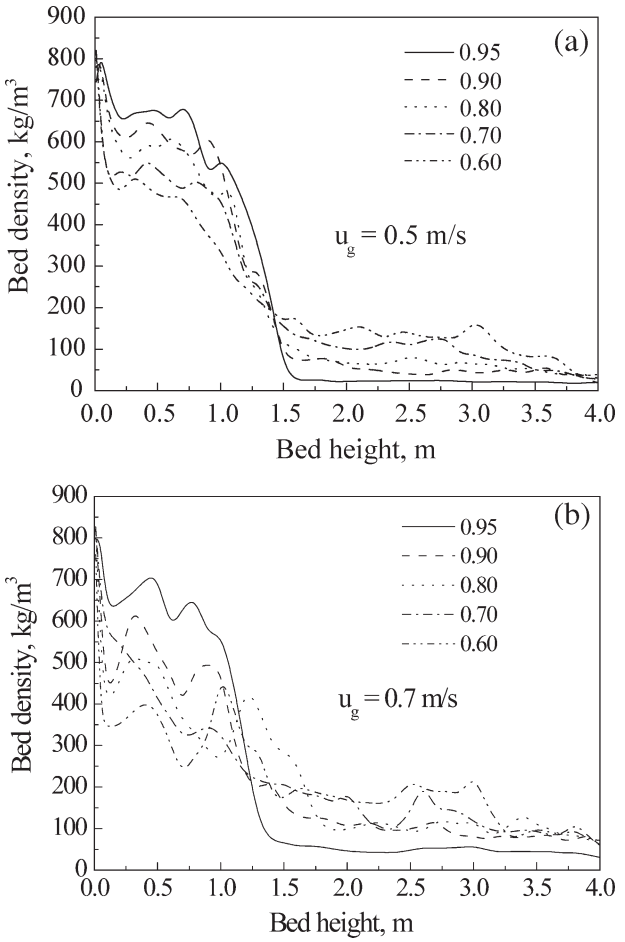

Figure 10. (a) Axial-bed density profile for various restitution coefficients (u_g = 0.5 m/s). (b) Axial-bed density profile for various restitution coefficients (u_g = 0.7 m/s).

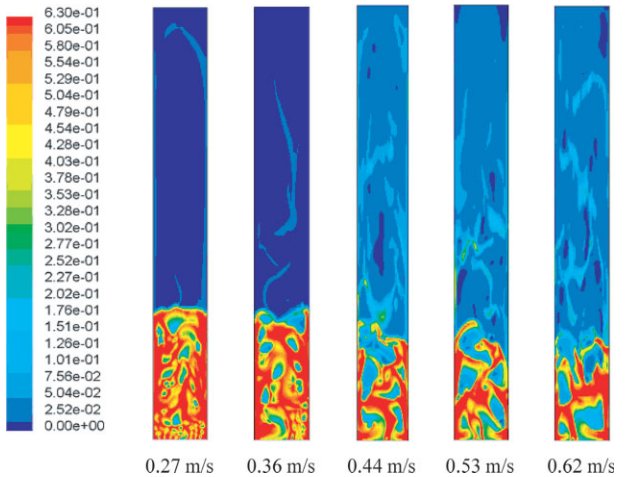

Figure 11. Instantaneous solid concentration profiles for various gas velocities.

[Color figure can be viewed in the online issue, which is available at www.interscience.wiley.com.]

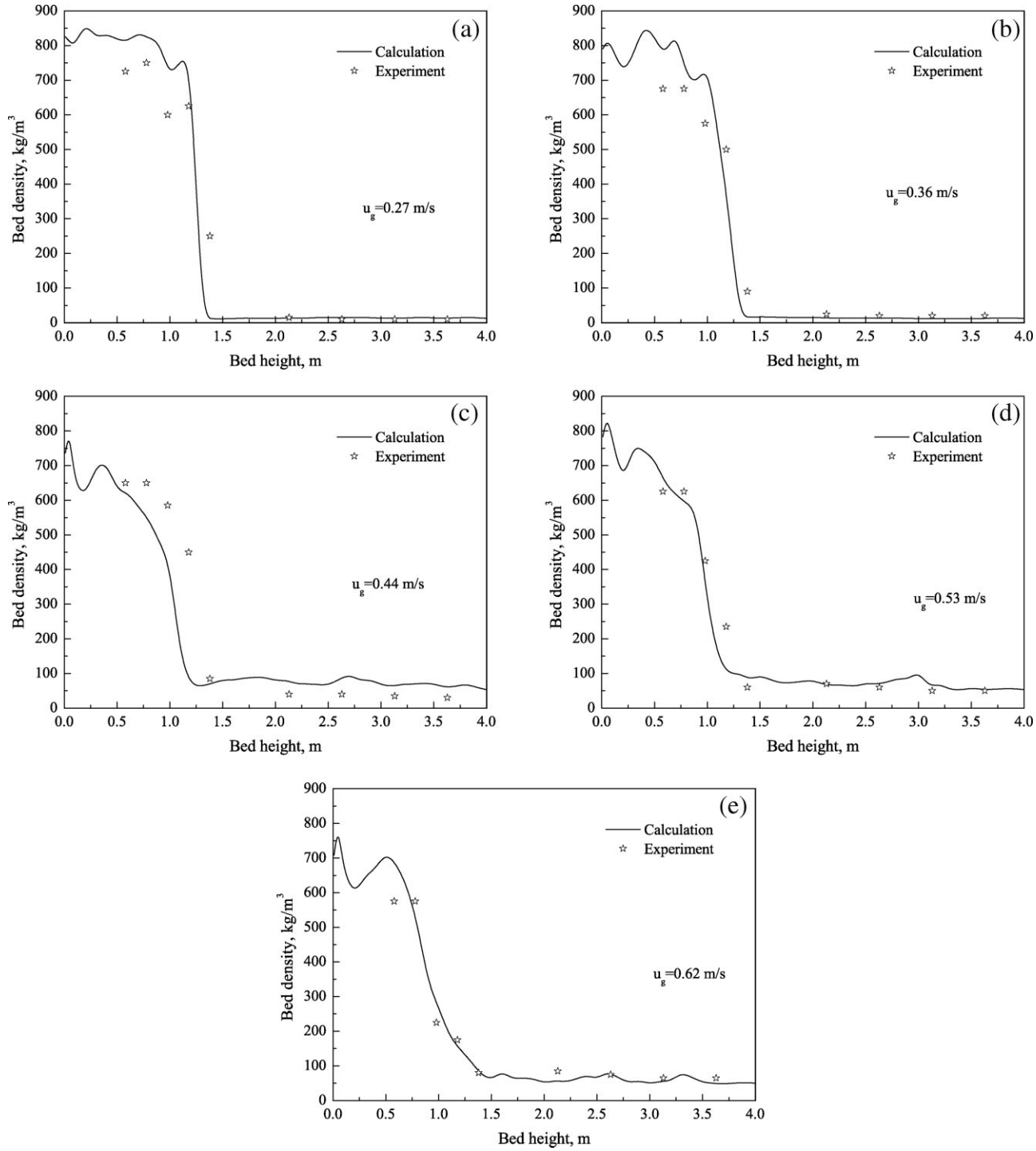

Figure 12. (a) Comparison of the predicted bed density with experimental results (u_g = 0.27 m/s); (b) comparison of the predicted bed density with experimental results (u_g = 0.36 m/s); (c) comparison of the predicted bed density with experimental results (u_g= 0.44 m/s); (d) comparison of the predicted bed density with experimental results (u_g = 0.53 m/s); (e) comparison of the predicted bed density with experimental results (u_g = 0.62 m/s).

model. In general, dense gas-solid multiphase flow in a bubbling or turbulent fluidized bed displays low Reynolds numbers, and the effect of the turbulent behavior, and the turbulent interaction between phases on the flow behavior is not very strong. Therefore, both the laminar and the turbulent models are suitable for predicting the hydrodynamics of the dense gas-solid flows. Almuttahar[38] found that even in the case of high-density circulating fluidized-bed riser, a laminar model presents a better hydrodynamics prediction than the turbulent model. In addition, unless an appropriate

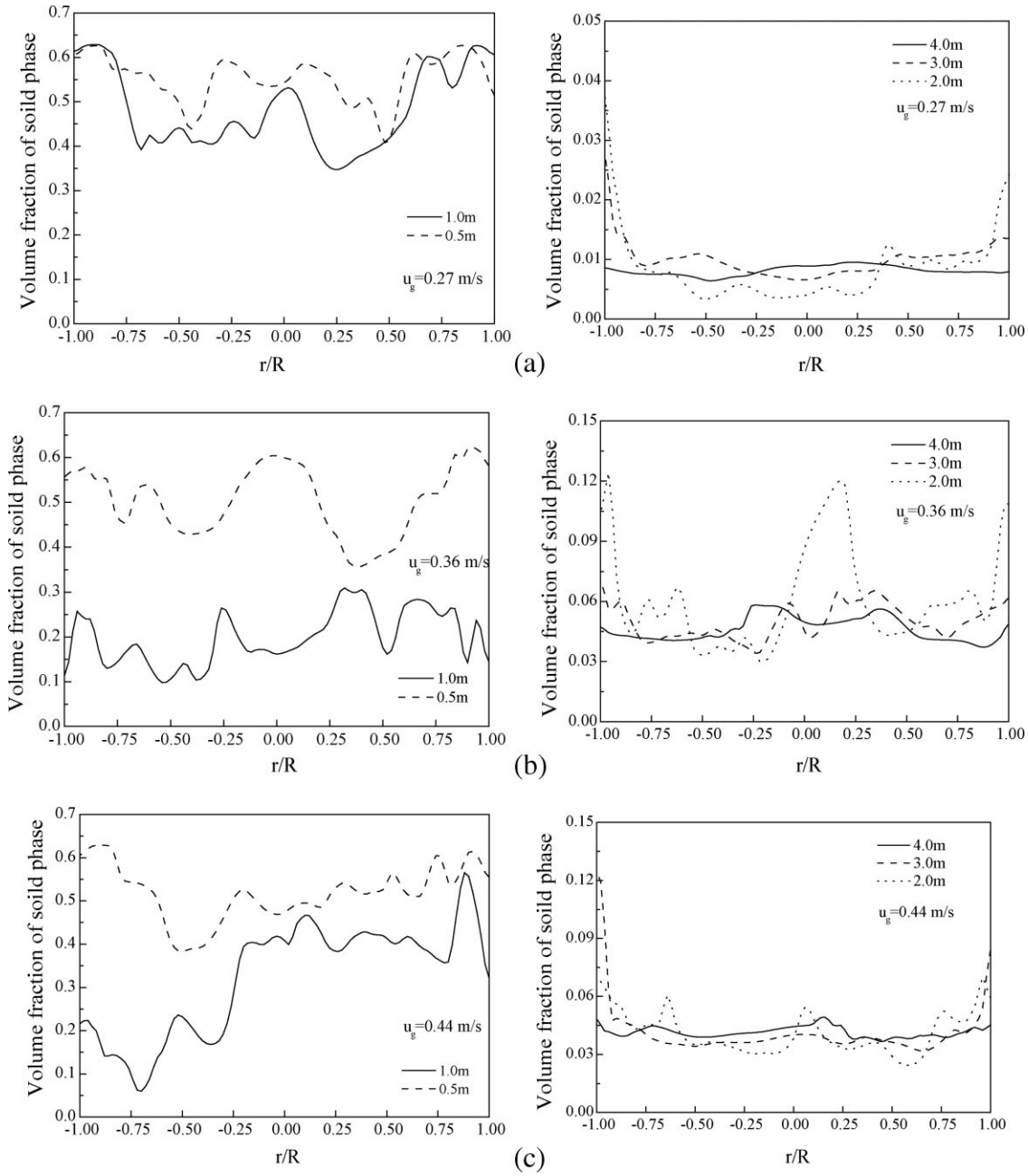

Figure 13. (a) Radial solid concentration distributions at different gas velocities (u_g = 0.27 m/s); (b) radial solid concentration distributions at different gas velocities (u_g = 0.36 m/s); (c) radial solid concentration distributions at different gas velocities (u_g = 0.44 m/s); (d) radial solid concentration distributions at different gas velocities (u_g = 0.53 m/s); (e) radial solid concentration distributions at different gas velocities (u_g = 0.62 m/s).

turbulence model with the correct empirical constants and closures is chosen, the turbulent model predictions may be less consistent than the laminar model.

Gidaspow kinetic theory vs. Syamlal-O'Brien kinetic theory

FLUENT software provides two kinds of kinetic theory (the Gidaspow[14] and Syamlal-O'Brien[15] kinetic theory) to calculate the collisional viscosity and kinetic viscosity part of solids-shear stresses, and the diffusion coefficient for granular energy in granular temperature equation. The effects of these two kinds of kinetic theory on the predicted hydrodynamics in the turbulent fluidized bed are investigated. The predicted axial bed density with these two kinetic theories is shown in Figure 9 for a gas velocity of 0.5 m/s.

It can be seen that there are no significant difference in the bed density predicted by the Gidaspow or Syamlal-O'Brien kinetic theory. The Gidaspow kinetic theory, however, is helpful for the convergence, and is therefore applied in the following simulation.

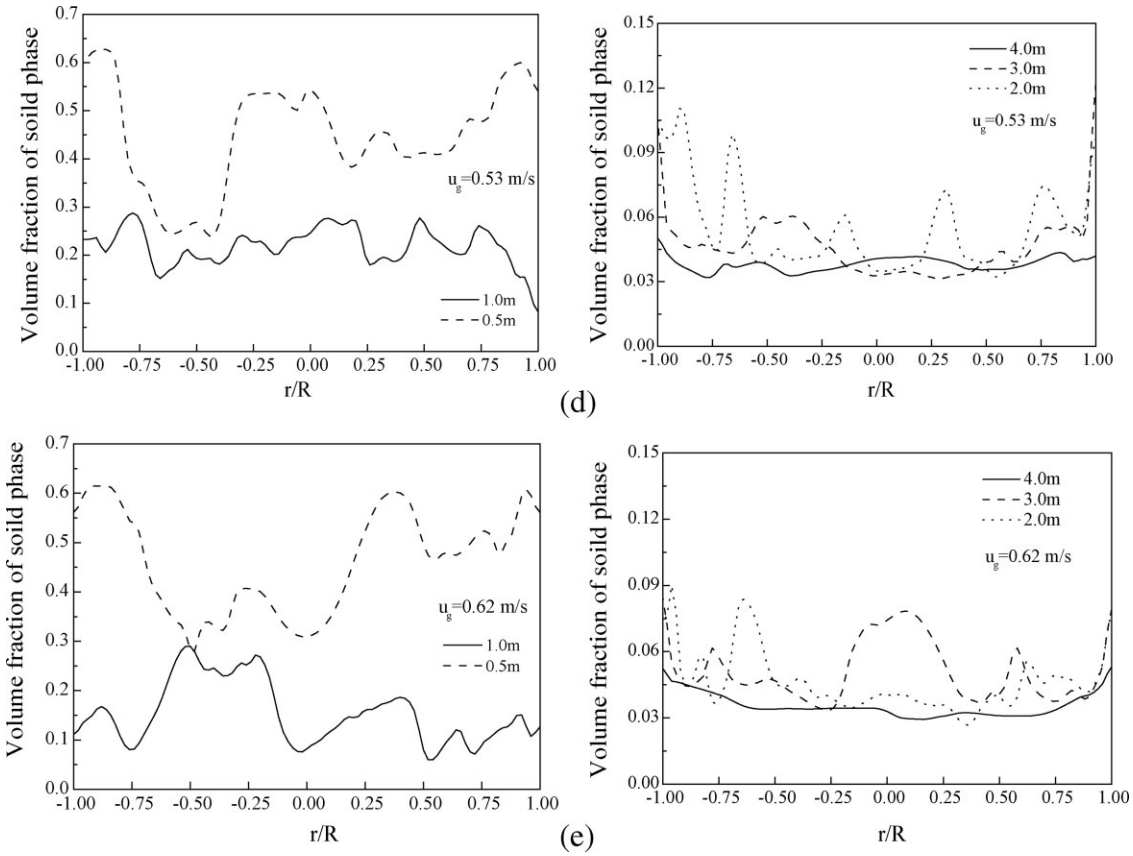

Figure 13. (Continued)

Effect of the coefficient of restitution

In addition to the drag force model, the flow behavior may be influenced by inelastic interparticle collisions resulting in kinetic energy dissipation. The restitution coefficient represents the elasticity of particle collisions and ranges from fully inelastic ($e = 0$) to fully elastic ($e = 1$). Some researchers reported that in the kinetic theory model there is a degree of sensitivity to the coefficient of restitution;[39] however, a different response of no significant changes[21] observed in the bubbling-bed behavior and the bed expansion for FCC particles at restitution coefficients from 0.6 to 0.99. This large difference in results shows the difficulty in determining the restitution coefficient for small particles such as FCC catalysts.

To confirm the effect of the restitution coefficient, a comparison of the axial bed density as a function of the coefficient of restitution is shown in Figure 10 for different superficial gas velocities.

With decreasing the value of restitution coefficient, the bed density of the dense phase decreases, while that in the dilute phase increases at each gas velocity. With the decrease of the restitution coefficient, the solid-phase shear viscosity and solid-bulk viscosity decrease in the kinetic theory of granular flows from the corresponding equations in Table 2. The decrease of solids-phase viscosity improves the fluidity of the FCC particle, resulting in more particles to be entrained into the dilute phase.

For a low value of restitution coefficient, the predicted bed density in dilute phase may be greater than 100 kg/m^3, which is inconsistent of the experimental data. As increasing the restitution coefficient from 0.90 to 0.95, the coexisting dilute and dense phase in the turbulent fluidized bed can be correctly predicted in all cases. Therefore, the restitution coefficient of 0.95 is used for the next simulation. The result above also indicated that the hydrodynamics shows a degree of sensitivity to the coefficient of restitution in a turbulent fluidized bed.

Comparison of Simulation and Experiment

Axial bed density profile

Figure 11 shows the instantaneous solid concentration in the fluidized bed at 30 s for various gas velocities. Figure 12 shows the comparison of average bed density in the axial direction between the simulated and experimental results. Predicted bed densities are drawn from the time-averaged values over the period of 25–30 s.

Figure 11 and 12 illustrate that there exist two different coexisting regions: a bottom dense, bubbling region and a dilute, dispersed flow region, which is consistent with the experiment in the turbulent fluidized bed. Moreover, the predicted bed density profile in the axial direction is in reasonable agreement with experimental results.

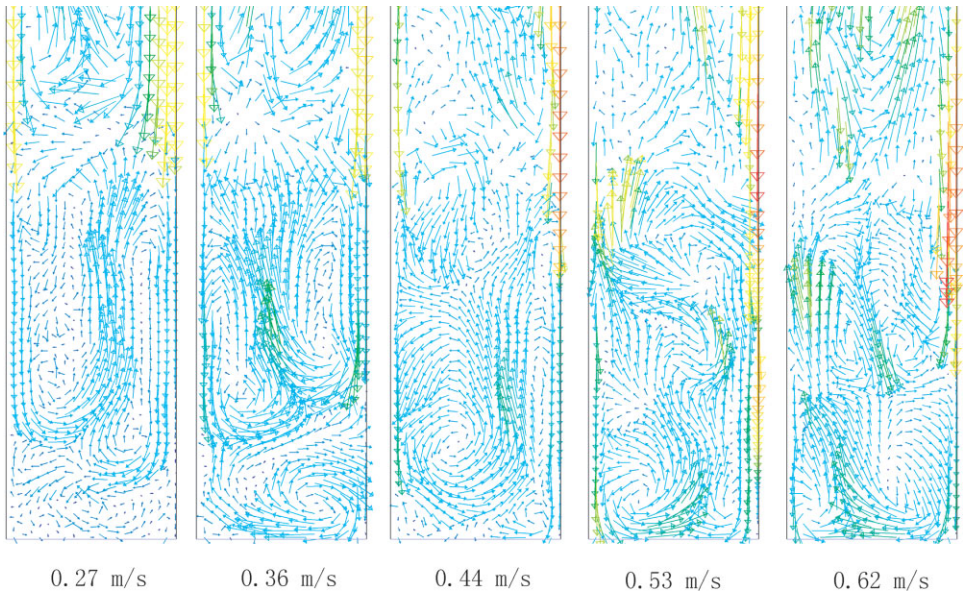

Figure 14. Instantaneous velocity vector profiles of particle phase in the dense phase.

[Color figure can be viewed in the online issue, which is available at www.interscience.wiley.com.]

It can be also seen that with increasing superficial gas velocity, the turbulence degree aggravates, and the entrainment capacity of gas-phase improves. More particles are entrained into the dilute phase region of the bed. Thus, the height and average density of the dense phase decrease, while the average density in the dilute phase increases.

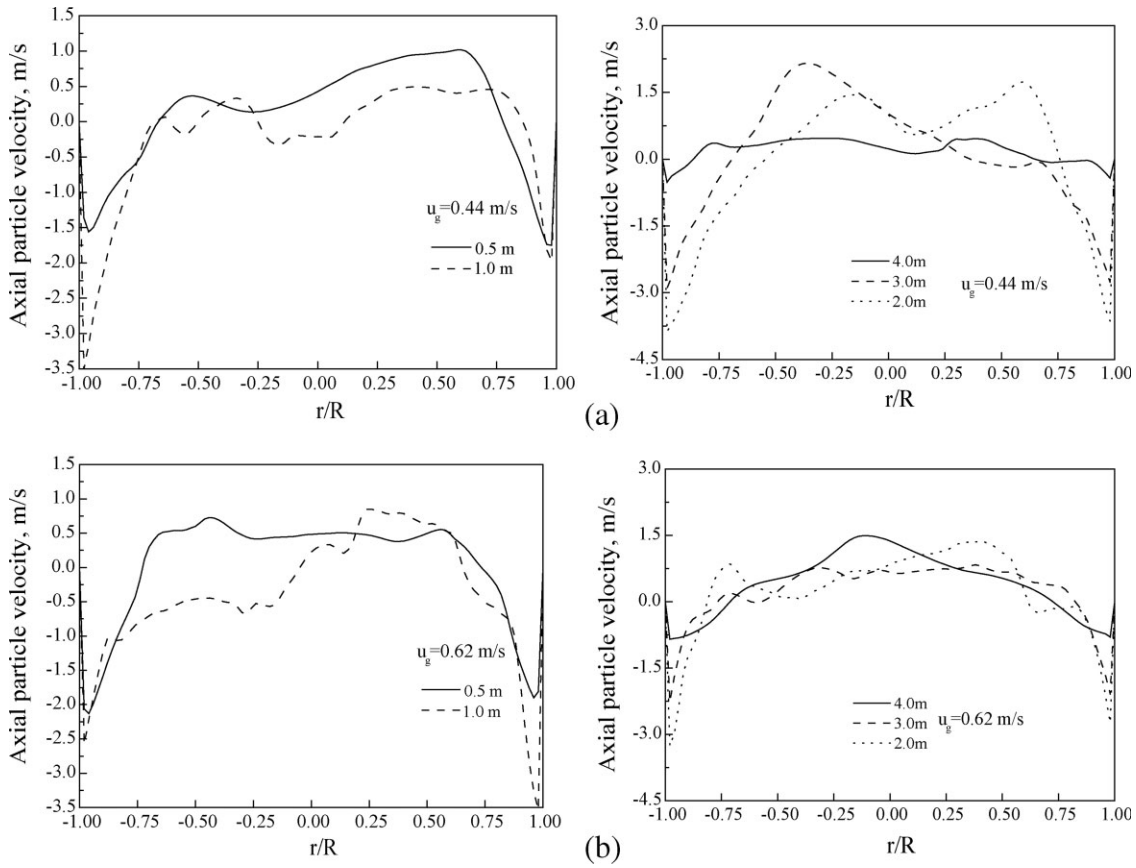

Figure 15. (a) Radial distributions of the axial particle velocities at different bed heights and gas velocities (u_g = 0.44 m/s). (b) Radial distributions of the axial particle velocities at different bed heights and gas velocities (u_g = 0.62 m/s).

Radial solid volume fraction profile

Figure 13 shows the radial particle concentration distributions at the bed heights of 0.5, 1.0, 2.0, 3.0 and 4.0 m and different superficial gas velocities. It can be found that solid volume fraction decreases with increasing bed height. At low-gas velocity of 0.27 m/s, the solid volume fractions show high near the wall region, and low in the center of the bed due to the effect of the wall on the gas-solid flow. The solid-volume fraction at the wall region approximates the maximum packing limit, which indicates a bad flow situation. The solid-volume fraction fluctuates drastically in the radial direction, showing the effect of the split and coalescence of the ascending bubbles.

As the gas velocity increase to 0.36 m/s, the solid volume fraction profile at the bottom of the bed (0.5 m) is similar to the case of 0.27 m/s. At the bed height of 1.0 m, however, the solid-volume fraction decreases, although fluctuating in the radial direction. Furthermore, the turbulence of the flow aggravates with increasing gas velocity. Solid-volume fractions show irregular in the radial direction of the bed except for the bottom zone of the bed (0.5 m).

Particle velocity profile

Figure 14 shows the transient velocity vector profiles of the particle phase in the dense phase of the fluidized bed (<1.5 m height). Figure 15 shows the axial particle velocity profiles at different bed heights and gas velocities as a function of the radial position. It can be seen that particles ascend in the center and descend at the wall region in the turbulent fluidized bed. Such flow patterns are related to the formation, motions and split of bubbles. Bubbles entraining particles with them move up in the center of the fluidized bed. When arriving at the fluidized-bed surface, bubbles breakup and release the particles within them. Particles then fall downward along the wall. In addition, vortex flows appear in the local position of the bed. The flow behavior shows turbulent disorder, resulting in the irregularity of particle concentration in radial direction.

Conclusion

Based on the effective mean diameter of particles clusters together with the bed voidage profile, a modified drag model has been proposed in this article. The dynamic characteristics of the gas-solids flow behavior in a turbulent fluidized bed were investigated by the CFD method incorporating this modified drag model. Relative to other drag models, the modified one gives a reasonable hydrodynamic prediction in comparison with experimental data in a turbulent fluidized bed.

Both the laminar and turbulent models are suitable for predicting the hydrodynamics of gas-solid flow behavior in turbulent fluidized bed. Moreover, a laminar model presents a better hydrodynamics prediction than the turbulent model.

The hydrodynamics shows a degree of sensitivity to the coefficient of restitution in a turbulent fluidized bed. With a restitution coefficient of 0.95, the coexisting dilute and dense phase in the turbulent fluidized bed can be correctly predicted. There are no significant differences in the bed density predicted by the Gidaspow or Syamlal kinetic theory.

Experimental and numerical results indicate that there exist two different coexisting regions: a bottom dense, bubbling region and a dilute, dispersed flow region in the turbulent fluidized bed. With increasing superficial gas velocity, the height and average density of the dense phase decrease, while the average density in the dilute phase increases.

At low-gas velocity, solid-volume fractions show high near the wall region and low in the center of the bed. Increasing gas velocity aggravates the turbulence degree of the flow. The flow behavior shows turbulent disorder, resulting in the irregularity of particle concentration in radial direction.

Acknowledgements

The authors acknowledge the supports by the National Natural Science Foundation of China through the programs for Distinguished Young Scholars of China (Grant No. 20725620 and Grant No. 20525621), and the programs "Multiple Scale Analysis and Scaling-up of Direct Coupled Dual Gas-Solid Fluidized Reaction Systems" (Grant No.20490202).

Notation

C_D = drag coefficient
d = diameter of particle, μm
d_p^* = effective mean diameter of particle, μm
e = restitution coefficient
g_i = acceleration due to gravity, m/s^2
g_0 = radial distribution function
h = bed height, m
p = pressure, Pa
r = radial direction
R = diameter of bed, mm
Re_p = particle Reynolds number
Re_p^* = cluster Reynolds number
t = time, s
u = velocity, m/s
u' = instantaneous turbulent component of velocity, m/s
U_0 = superficial gas velocity, m/s
u_t = terminal velocity, m/s
u_t^* = experimental terminal velocity, m/s
x = direction coordinate

Greek letters

α = volume fraction
α_i = void fraction for the dividing criteria
β = interphase momentum exchange coefficient kg/(m^3·s)
γ = collisional dissipation of energy fluctuation, kg/(m^3· s)
ξ_p = solid-bulk viscosity, Pa·s
Θ = granular temperature, m^2/s^2
μ = solid-phase shear viscosity, Pa·s
ρ = density, kg/m^3
ϕ = switch function
τ = stress tensor, Pa
Γ_Θ = diffusion coefficient for the energy fluctuation, kg/(m·s)

Subscripts

i, j, k = direction coordinate
g = gas-phase
max = maximum
p = particulate phase

Literature Cited

1. Jiradilok V, Gidaspow D, Damronglerd S, Koves WJ, Mostofi R. Kinetic theory based CFD simulation of turbulent fluidization of FCC particles in a riser. *Chem Eng Sci*. 2006;61:5544–5559.

2. Berruti F, Chaouki J, Godfroy L, Pugsley TS, Patience GS. Hydrodynamics of circulating fluidized bed risers: a review. *Can J Chem Eng*. 1995;73:579–602.
3. Lu CM. *Hydrodynamics of circulating turbulent fluidized bed in FCC regeneration*. China University of Petroleum: P.R. China; 1996. PhD thesis.
4. Bi HT, Ellis N, Abba IA, Grace JR. A state-of-the-art review of gas-solid turbulent fluidization. *Chem Eng Sci*. 2000;55:4789–4825.
5. Du B, Warsito W, Fan LS. Nonhomogeneity in turbulent gas-solid fluidization. *AIChE J*. 2003;49:1109–1126.
6. Grace JR. Reflections on turbulent fluidization and dense suspension upflow. *Powder Technol*. 2000;113:242–248.
7. Andreux R, Gauthier T, Chaouki J, Simonin O. New description of fluidization regimes. *AIChE J*. 2005;51:1125–1130.
8. Du B, Fan LS, Wei F, Warsito W. Gas and solids mixing in a turbulent fluidized bed. *AIChE J*. 2002;48:1896–1909.
9. Ellis N, Bi HT, Lim CJ, Grace JR. Hydrodynamics of turbulent fluidized beds of different diameters. *Powder Technol*. 2004;141:124–136.
10. Cao B, Gao JS, Zhang P, Zheng XJ, Xu CM. Numerical Simulation on the Gas-Particle Flows in FCC Regenerator. *The Second International Symposium on Multiphase, Non-Newtonian and Reacting Flows'04*. Hangzhou, China; 2004.
11. Sinclair JL, Jackson R. Gas-particle flow in a vertical pipe with particle-particle interactions. *AIChE J*. 1989;35:1473–1496.
12. Gidaspow D. *Multiphase Flow and Fluidization: Continuum and Kinetic Theory Description*. Boston: Academic Press; 1994.
13. FLUENT6.2.16, User's Guide, FLUENT, Inc.; 2006
14. Gidaspow D, Bezburuah R, Ding J. Hydrodynamics of Circulating Fluidized Beds, Kinetic Theory Approach. In: Fluidization VII, Proceedings of the 7th Engineering Foundation Conference on Fluidization, Brisbane 1992;75–82.
15. Syamlal M, Rogers W, O'Brien TJ. MFIX Documentation: Volume 1, Theory Guide. National Technical Information Service, Springfield, VA, 1993. DOE/METC-9411004, NTIS/DE9400087.
16. Ergun S. Fluid flow through packed columns. *Chem Eng Progr*. 1952;48:89–94.
17. Richardson JF, Zaki WN. *Sedimentation and fluidization: part 1. Trans Am Inst Chem Eng*. 1954;32:35–53.
18. Syamlal M, O'Brien TJ. *The derivation of a drag coefficient formula from velocity-voidage correlations*. U.S. Department of Energy, Office of Fossil Energy, Technical Report; 1994.
19. Wen CY, Yu YH. Mechanics of fluidization. *Chem Eng Prog Symp Ser*. 1966;62:100–110.
20. Zimmermann S, Taghipour F. CFD modeling of the hydrodynamics and reaction kinetics of FCC fluidized-bed reactors. *Ind Eng Chem Res*. 2005;44:9818–9827.
21. McKeen T. Pugsley T. Simulation and experimental validation of a freely bubbling bed of FCC catalyst. *Powder Technol*. 2003;129:139–152.
22. Qi H, You C. Boemer A. Renz U. Eulerian Simulation of Gas-Solid Two-Phase Flow in a CFB-Riser under Consideration of Cluster Effects. In: *Fluidization 2000: Science and Technology*. Xu D., Mori S, eds. Xi'an Publishing House: Xi'an, China; 2000.
23. O'Brien TJ, Syamlal M. Particle cluster effects in the numerical simulation of a circulating fluidized bed. In *Preprint Volume for CFB-IV*. Avidan AA, ed. AIChE; New York; 1993:430–435.
24. Syamlal M, O'Brien TJ. Fluid dynamic simulation of O_3 decomposition in a bubbling fluidized. *AIChE J*. 2003;49:2793–2801.
25. Hulme I, Clavelle E, van der Lee L, Kantzas A. CFD modeling and validation of bubble properties for a bubbling fluidized bed. *Ind Eng Chem Res*. 2005;44:4254–4266.
26. Yang N, Wang W, Ge W, Li JH. CFD simulation of concurrent-up gas-solid flow in circulating fluidized beds with structure-dependent drag coefficient. *Chem Eng J*. 2003;96:71–80.
27. Yang N, Wang W, Ge W, Wang LN, Li JH. Simulation of heterogeneous structure in a circulating fluidized-bed riser by combining the two-fluid model with the EMMS approach. *Ind Eng Chem Res*. 2004;43:5548–5561.
28. McKeen T, Pugsley T. Simulation of Cold Flow FCC stripper hydrodynamics at small scale using computational fluid dynamics. *Int J Chem Reactor Eng*. 2003;1:A18.
29. Sharma SD, Pugsley T, Delatour R. Three-dimensional CFD model of the deaeration rate of FCC particles. *AIChE J*. 2006;52:2391–2400.
30. Gibilaro LG, Di Felice R, Waldram SP. Generalized friction factor coefficient correlations for fluid-particle interactions. *Chem Eng Sci*. 1985;40:1817–1823.
31. Arastoopour H, Gidaspow D. Analysis of IGT pneumatic conveying data and fast fluidization using a thermohydrodynamic model. *Powder Technol*. 1979;22:77–87.
32. Lettieri P, Newton D, Yates JG. Homogeneous bed expansion of FCC catalysts, influence of temperature on the parameters of the Richardson-Zaki equation. *Powder Technol*. 2002;123:221–231.
33. Matsen JM. Mechanisms of choking and entrainment. *Powder Technol*. 1982;32:21–33.
34. Matsen JM. Drift flux representation of gas-particle flow. *Powder Technol*. 2002;111:25–33.
35. Schiller L, Naumann A. A drag coefficient correlation. *VDI Zeits*. 1933;77:318–320.
36. Lu HL, Gidaspow D. Hydrodynamics of binary fluidization in a riser: CFD simulation using two granular temperatures. *Chem Eng Sci*. 2003;58:3777–3792.
37. Patankar SV. *Numerical Heat Transfer and Fluid Flow*. Hemisphere Publishing Corp; 1980
38. Almuttahar A, Taghipour F. Computational fluid dynamics of high density circulating fluidized bed riser: Study of modeling parameters. *Powder Technol*. 2008;185:11–23.
39. Goldschmidt M, Kuipers J, Swaaij WM. Hydrodynamic modeling of dense gas-fluidized beds using the kinetic theory of granular flow: Effect of coefficient of restitution on bed dynamics. *Chem Eng Sci*. 2001;56:571–578.

Manuscript received May 8, 2008, and revision received Dec. 18, 2008.